Journal of proteome research

TECHNICAL NOTE

pubs.acs.org/jpr

Integrated Analysis of ATM Mediated Gene and Protein Expression Impacting Cellular Metabolism

Amrita K. Cheema,[*,†,‡] Olga Timofeeva,[†,‡] Rency Varghese,[‡] Alexandre Dimtchev,[∥] Kathryn Shiekh,[‡] Vladimir Shulaev,[§] Simeng Suy,[‡] Sean Collins,[‡] Habtom Ressom,[‡] Mira Jung,[∥] and Anatoly Dritschilo[‡,∥]

[‡]Departments of Oncology and [∥]Radiation Medicine, Lombardi Comprehensive Cancer Center at Georgetown University Medical Center, Washington, D.C., United States

[§]Virginia Bioinformatics institute, Blacksburg, Virginia, United States

Supporting Information

ABSTRACT: A major goal of systems biology is to decipher cellular responses to genetic perturbations or environmental changes. Network integration of high-throughput data sets such as transcriptomics, proteomics, and metabolomics ("3-omics") offers a powerful tool for understanding the regulation and organization of cellular functions and biological processes. Given that the *ATM* (the product of the ataxia-telangiectasia mutated) gene exhibits multifaceted functions involved in complex biological networks, we attempted to analyze "3-omics" data sets by utilizing a functional pathway analysis approach. ATM-mediated gene and protein expression and metabolite products were interrogated using a model system comprised of cells genetically similar but demonstrating ATM deficiency (AT5BIVA) or ATM proficiency (ATCL8). Here, we report an unprecedented finding from the results of this integrated analysis revealing that ATM dictates purine, pyrimidine, and urea cycle pathways through the regulation of adenosine monophosphate (AMP) activated protein kinase (AMPK), a major sensor and regulator of cellular energy homeostasis. Furthermore, our results support the feasibility of applying a systems approach for identification of specific cellular networks and understanding of pathway perturbations underlying the complex A-T clinical syndrome.

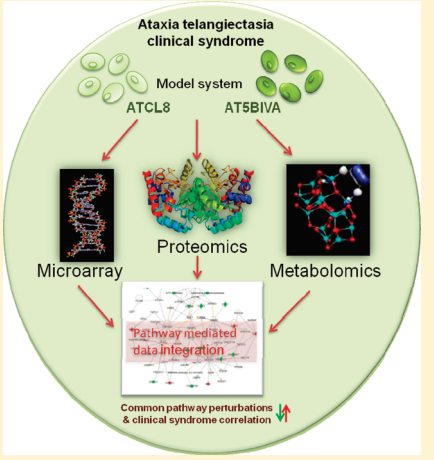

KEYWORDS: metabolomics, transcriptomics, integromics, systems biology

INTRODUCTION

Technological advances in mass spectrometry have enabled us to detect chemically and structurally diverse classes of endogenous small molecule metabolites that participate in various biochemical pathways.[1] The value of metabolomic profiling of biological samples, as a high throughput, cost-effective and a minimally invasive diagnostic tool in a clinical setting, is fast gaining credence.[2] However, to obtain a mechanistic understanding of a disease and its progression, the integration of transcriptomics and proteomics data provide complementary information for co-ordination and reconstruction of interactive metabolic networks.[3−5] Moreover, the resultant predictive models offer promise toward drug discovery, improving industrial processes and the predictive, preventive, personalized and participatory (P4) medicine paradigm, which seeks to focus on dynamics, interaction and malfunction of cellular networks to understand the molecular basis of disease development.[6,7]

In this study, we used a genetically defined model cell system which consists of cells expressing a kinase dead and a kinase proficient ATM gene product. Ataxia telangiectasia (A-T) is a human autosomal recessive genetic disorder clinically characterized by cerebellar ataxia, cutaneous telangiectasias, immunodeficiency, extreme radiosensitivity and predisposition to cancer.[8−11] The A-T clinical syndrome is a consequence of mutation in the *ATM* gene leading to loss of the functional kinase, the chief activator of the cellular response to DNA double strand breaks.[12−14] This results in cell cycle dysregulation, apoptosis and defective responses to oxidative stresses.[15] Other abnormalities, such as neurodegeneration and immune-system defects, are believed to arise as a consequence of unrepaired DNA breaks, leading to cell death, or indirectly, as a response to the build-up of oxidative stress in the presence of persistent DNA breaks. Studies of the ATM gene product have revealed a complex set of functions that primarily lead to target protein post-translational modifications activating signaling pathways and protecting against genome instability to reduce the risk of cancer. Using this model cell system, we previously reported ATM-dependent metabolic responses to radiation exposure.[16]

Since genetic modification is expected to result in alteration of molecular networks, we set out to determine the correlation of gene and protein expression with the quantitative metabolic profiling data obtained using the isogenic model cell system as outlined in Figure 1. Our results show common underlying

Received: December 15, 2010
Published: February 15, 2011

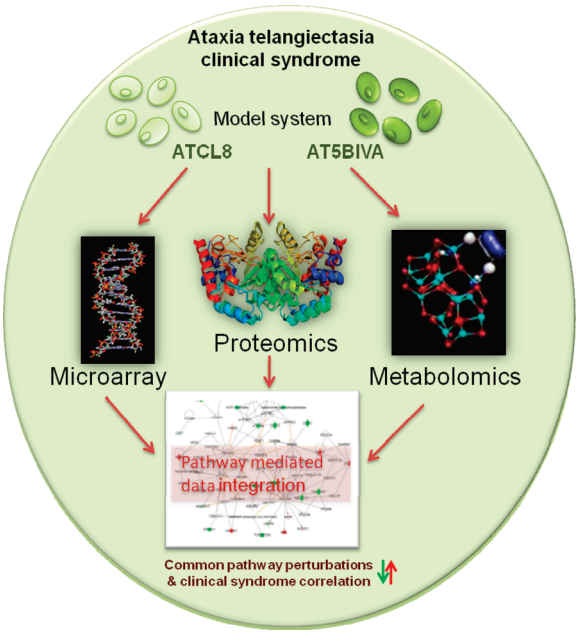

Figure 1. Overall workflow for global integrated analysis using an isogenic model cell system. The parental AT5BIVA cells (ATM deficient) were stably transformed with wild-type full-length ATM to generate ATCL8 (ATM proficient) cells. These cells were subjected to transcriptomic, proteomic, and metabolomic analysis. The resultant data were scored for common pathway perturbations using the ingenuity pathway analysis tool.

pathway perturbations in response to disruption of ATM function and underscore the feasibility of a functional pathway analysis approach for future studies with an integrated system focus. We further demonstrate that the changes in the levels of adenosine monophosphate (AMP) participating in purine metabolism were dependent on the functional status of ATM in the cell, which in turn altered the AMPK pathway, a chief regulator of cellular homeostasis.

MATERIALS AND METHODS

Compounds

The following compounds were purchased from Sigma, St. Louis, MO: xanthine, adenosine, adenosine monophosphate, adenosine triphosphate, alloxanthine, guanine, adenine, Uridine monophosphate, guanosine monophosphate, L-Glutamate, Uridine, spermidine, beta-alanine. All solvents used for LC−MS analysis and sample preparation, were LC−MS grade (Fisher Scientific, Pittsburgh, PA—Optima grade).

Cell Cultures

Ataxia telangiectasia fibroblast cells AT5BIVA, AT3BIVA, AT4BIVA, and MRC5CV1 cells were obtained from the National Institute of General Medical Sciences (NIGMS). Cells were maintained in modified Eagle's medium with 20% fetal bovine serum, 100 U/penicillin, and 100 pg/mL streptomycin. The ATCL8 cell line was established by transfecting AT5BIVA cells with the wild type, full length "ATM" cDNA in a pCDNA expression vector and selected by screening for correction of radiation sensitivity.[17] For this study the cells were grown to 80% confluence and serum starved for 24 h. The cells were then washed twice with chilled phosphate buffered saline (PBS) and harvested by scraping and centrifuging. Total cell counts were determined using a hemocytometer, and an equal numbers of cells (10^7) from each time point were aliquoted for proteomic and metabolomic analyses.

Clonogenic Cell Survival Assays

Logarithmically growing cells were exposed to graded doses of gamma-radiation in air at room temperature using a [137Cs] irradiator (J.L. Shepard Mark I). Cells were grown for three weeks for colony formation and stained with crystal violet. Colonies containing 50 or more cells were counted and radiation clonogenic survivals were obtained by fitting the single hit multitarget survival model. Experiments were performed in triplicate and the data points are plotted as the mean ± SEM on semilogarithmic plots for each experiment.

Affymetrix Microarray Analysis

Total RNA extracts were obtained using an RNeasy kit (Qiagen, Valencia, CA). RNA labeling and hybridization were performed according to the Affymetrix protocol for one-cycle target labeling. For each experiment, fragmented cRNA was hybridized in triplicates to Affymetrix GeneChip HG-U95Av2 array (Affymetrix, Santa Clara, CA), which represents approximately 10 000 full-length genes. Affymetrix data analysis included preprocessing of the probe-level Affymetrix data (CEL files). We applied RMA for background adjustment, quantile method for normalization, and the "median polish" for summarization. The triplicate arrays, performed in duplicates, representing the same subject were averaged. We selected the probe sets with significant differences in their expression levels based on a false discovery rate ≤ 0.05 and fold change ≥ 1.5. Pathway analysis was performed with Database for Annotation, Visualization and Integrated Discovery (DAVID).[18] Additionally, the data set was also analyzed using the ingenuity pathway analysis (IPA) tool.

Quantitative RT-PCR

Total RNA was reverse-transcribed using the High Capacity cDNA Reverse Transcription Kit (Applied Biosystems). Quantitative real-time PCR (qRT-PCR) was performed as two independent experiments in triplicates, using TaqMan Gene Expression Assays (Applied Biosystems) on the Applied Biosystems 7900HT Fast Real-time PCR System. Amplification of 18S rRNA provided an endogenous control to standardize the amount of sample added to the reaction. The comparative cycle threshold (CT) method was used to analyze the data by generating relative values of the amount of target cDNA (Applied Biosystems). CT represents the number of cycles for the amplification of target to reach a fixed threshold and correlates with the amount of starting material present. To obtain relative values, the following arithmetic formula was used: $2-\Delta\Delta CT$, where ΔCT = difference between the threshold cycles of the target and an endogenous reference (18S), and $-\Delta\Delta CT$ = difference between ΔCT of the target sample (ATCL8) and a designated calibrator (AT5BIVA). The statistical analyses of these data were performed with a two-sided *t* test since the expression data showed normal distribution.

siRNA Knockdown

Stealth RNAi (RNAi) to silence the expression of ATM and nonspecific Block-it RNA were obtained from Invitrogen (Carlsbad, CA). The controls included nonsilencing Cy3-labeled siRNA and Cy3-labeled GAPDH siRNA, obtained from Qiagen (Austin, TX). ATCL8 and MRC5CV1 cells were transfected with 10−50 nM siRNA. Transfection was performed using

Trans-TKO reagent from Mirus (Madison, WI) according to the manufacturer's instructions. Total RNA and protein were extracted 24, 48, and 72 h after transfection. The ATM mRNA levels were measured by qRT-PCR using TaqMan Gene Expression Assays (Applied Biosystems) on the Applied Biosystems 7900HT Fast Real-time PCR System using standard mode as described above.

Two-Dimensional Gel Electrophoresis and Protein Staining

For proteomics experiments, two 2D gels were run for each of the three biological replicates per cell type to yield six independent data sets. Five-hundred micrograms of each prepared whole cell lysate were loaded onto IPG ReadyStrips pH 3−10 NL (Bio-Rad), and rehydrated at 50 V for 12 h at 20 °C. Isoelectric focusing on the Protean IEF Cell from Bio-Rad was performed as follows: 15 min at 250 V, a rapid voltage ramping to 10 000 V, and a final step at 10 000 V up to 80 000 Vhours. The strips were equilibrated and the proteins were resolved on a second dimension on 12% SDS-PAGE gels, fixed and stained with commassie blue G250, destained in water and imaged. The Protein patterns were compared using Dymension imaging software (version 1.5, Syngene). Each of the 2D gels was used for comparison of spot density. For a protein spot to qualify as a differentially expressed spot high stringency cutoff parameters were used. Spots with a fold change of ≥ 2 with p value ≤ 0.05 were considered to be statistically significant and were subsequently selected for identification by mass spectrometry.

In-Gel Tryptic Digestion and Protein Identification by Mass Spectrometry

Briefly, the protein spots of interest were manually excised from the 2D-gel, transferred to Montage plate (Millipore) and destained with 50% acetonitrile in 25 mM ammonium bicarbonate, dehydrated with acetonitrile for 5 min, and vacuum-dried. Gel pieces were then rehydrated with 25 mM ammonium bicarbonate supplemented with trypsin (5 ng/μL, Promega, Madison, WI) at 37 °C for 16hrs. Subsequently, tryptic peptides were extracted in 0.1%TFA/50% acetonitrile and mixed with equal volume of 5 mg/mL CHCA (Acros Organics, Fair Lawn, NJ). Mass spectra were recorded with a matrix assisted laser desorption/ionization−time-of-flight, time-of-flight (MALDI-TOF-TOF) spectrometer (4700 Proteomics Analyzer, Applied Biosystems, Foster City, CA) set in reflector positive mode by spotting the samples onto a MALDI plate. Peptide masses were compared with the theoretical masses derived from the sequences contained in Swiss-Prot databases using MASCOT. The search parameters were set as follows: cysteines as carbamidomethyl derivative, allowed peptide mass error 50−75 ppm, at least four peptides mass hits required for protein match, up to one missed cleavage and methionine oxidized form.

Ultraperformance Liquid Chromatography−Time-of-Flight Mass Spectrometry (UPLC−TOF MS) based Metabolomic Analyses

In metabolomics experiments, we performed three biological replicates for each cell type and acquired the TOF MS data in duplicates. The biological replicates were indicative of the biological variability during cell growth, harvesting and processing while the technical replicates measure the UPLC−MS performance for every injection. We found one injection to be slightly off for AT5BIVA; hence, we proceeded with data analysis using 5 sets of data per cell type. Metabolite extraction was performed as per the protocol described by Sheikh et al.[19] Briefly, the cell pellets were resuspended in 150ul of water and vortexed. The samples were incubated and plunged into dry ice for 30 s followed by a heat shock at 37 °C for 30 s. 600 ul of methanol containing 4, nitrobenzoic acid and debrisoquine were then added and the samples were vortexed, transferred to room temperature and extracted with chloroform. The tubes were transferred to −20 °C for overnight incubation and subsequently centrifuged at 4 °C for 10 min at 12 000 rpm. The top and bottom phases were transferred to different tubes carefully avoiding the middle interface (containing precipitated proteins). An equivalent amount of chilled acetonitrile (ACN) was then added and the samples cooled on ice for 15 min after vortexing. Samples were centrifuged at 4 °C for 10 min at 12 000 rpm and the supernatant was transferred to a fresh tube and dried under vacuum. The residual pellet was resuspended in 200 μL of solvent A (98% water, 2% ACN and 0.1% formic acid) for UPLC−TOF MS analysis and the data were acquired in duplicate (two technical replicates) for each sample.

Measurement of ATP in Cultured Cells

ATP was measured by using the ATP Determination Kit (Invitrogen, Carlsbad, CA) according to manufacturer's recommendations. To obtain statistically significant results, each sample was analyzed in duplicate for three independently performed experiments.

Western Blot Analyses

Anti-phospho-AMPK, AMPK, and antiphospho-ACC were purchased from Cell Signaling Technology and used at a dilution 1/1000. Cell lysates were prepared from AT5BIVA, ATCL8, MRC5CV1, AT3BIVA, and AT4BIVA grown in 10 cm culture dishes. For analysis of AMPK and ACC phosphorylation, cells were immediately scraped off into lysis buffer (1% Triton X-100 in 50 mM Hepes pH 7.4 at 4 °C, containing 50 mM NaF, 5 mM NaPPi, 1 mM EDTA, 1 mM EGTA, 10% glycerol and protease and phosphatase inhibitors). The protein contents of these samples were measured using the Bradford assay (Bio-Rad Laboratories) and 40 μg protein aliquots were used for PAGE separation and further transfer onto Immobilon-P membrane filters (Millipore). Antibody binding was detected with a horseradish peroxidase (HRP)-conjugated secondary antibody using the ECL detection system (Amersham Pharmacia Biotech). Protein loading was routinely confirmed with an antibody against β-actin (Sigma-Aldrich). Semiquantitative analysis was performed by calculating the densitometry ratios versus β-actin.

Ingenuity Pathway Analysis (IPA)

The microarray, proteomics and metabolomics data sets were analyzed using the IPA tool independently and also in an integrative manner to score for overlapping pathways of "3-omics" data sets.

RESULTS AND DISCUSSION

We established a genetically defined model cell system, by introducing a full-length ATM expressing vector into AT5BIVA fibroblasts, originally derived from a patient with A-T. A key phenotype of A-T, extreme cellular sensitivity to ionizing radiation, allowed for complementation-based selection of clonal cells (ATCL8) expressing a functional ATM. Relative radiation sensitivities of cells were used to identify ATCL8 cells, with a D_0 of 1.6 Gy, while the sensitive AT5BIVA parental cells have a D_0 of 0.8 Gy (Figure 2A).[17] Western analysis demonstrated characteristic triggering of ATM phosphorylation at serine 1981 one hour following exposure of cells to 5 Gy of ionizing radiation

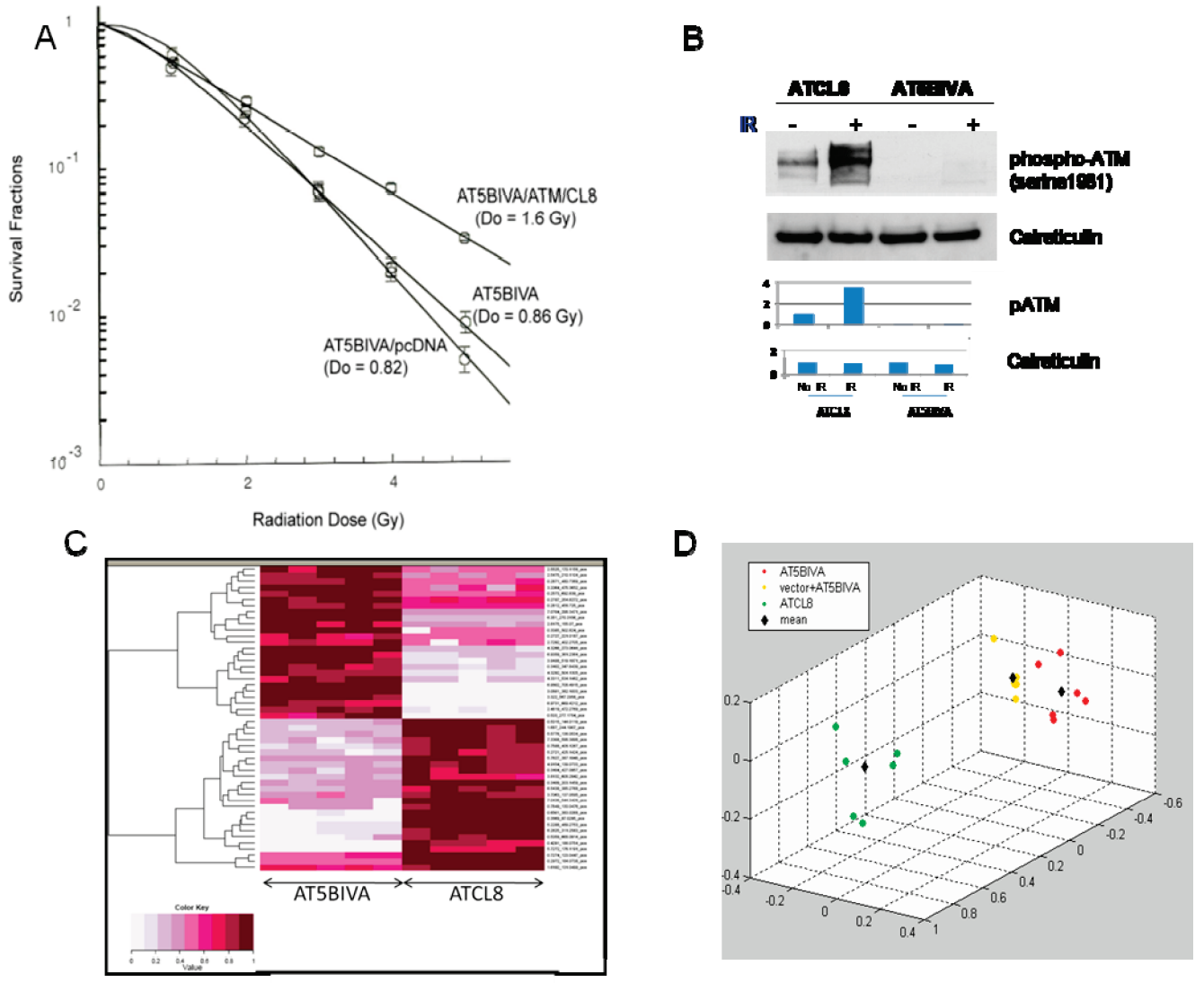

Figure 2. Characterization of model cell lines AT5BIVA and ATCL8 (panels A and B) and "omics" profiling (panels C and D). (A) Clonogenic assay to determine radiation sensitivity. (B) ATM activation through serine 1981 phosphorylation at 1 h following exposure to 5 Gy γ radiation in ATCL8 but not in AT5BIVA confirms the presence of functional ATM kinase in ATCL8 cells. (C) Heat map generated using the random forest software for metabolomic profiling, shows the expression of the top 50 differentially expressed metabolites in the two cell lines, respectively. Each row represents a feature with a characteristic mass/charge (m/z) and retention time value (see Supplementary Table S1, Supporting Information). The class separation is based on hierarchical clustering. (D) Multidimensional scaling plot of microarray profiling shows class separation of differentially expressed genes in different cell types.

in ATCL8, but not in AT5BIVA (Figure 2 B) confirming the presence of an activated ATM in ATCL8.[20]

Using this genetically defined model cell system, we asked whether perturbation in cellular ATM function causes changes in metabolic pathways, which may correlate with alterations of gene and protein expression profiles. As an outlined overall approach in Figure 1, the microarray, proteomics and metabolomics data were acquired and analyzed independently. These data were then integrated using the ingenuity pathway analysis tool (IPA) and scored for functional pathways exhibiting maximum correlation at all three levels of cellular expression.

Initially, to determine effects of ATM restoration on levels of metabolic products, metabolomic profiles were determined using the ultra performance liquid chromatography coupled with time-of-flight mass spectrometry (UPLC−TOF MS). The resultant 2700 positive and 1500 negative features were normalized to total protein concentration and the peak intensity of the internal standards. Orthogonal partial least-squares (OPLS) using the SIMCA-P software (Umetrics, Inc.) and the random forests algorithms[21] were used for multivariate data analysis. Feature rankings allowed identification of putative candidate biomarkers reflecting differences in metabolomic profiles (Supplementary Figure S1A, S1B, Supporting Information, and Figure 2C, Supplementary Table S1, Supporting Information, respectively). Accurate mass based search using the Madison Metabolomic Consortium Database (MMCD) and the human metabolome database (HMDB) yielded identifications of 315 metabolites showing fold changes ≥ 2 and p-values ≤ 0.05. These were selected for functional pathway analysis using the IPA, to score for the predominant canonical pathways affected by the change in the functional status of ATM (Supplementary Figure S2, Supporting Information).

dx.doi.org/10.1021/pr101243j |J. Proteome Res. 2011, 10, 2651–2657

Table 1. Integrated Functional Pathway Analysis Using the Ingenuity Pathway Analysis Tool for Correlating Basal Changes in Expression at the Transcriptomic, Proteomic, and Metabolomic Levels

	Genes			Proteins				Metabolites		
Pathway	Symbol	Description	ATCL8/ AT5BIVA	Symbol	Decription	Acc ID	ATCL8/ AT5BIVA	Name	Kegg ID	ATCL8/ AT5BIVA
Purine Metabolism	ABCC1	ATP-binding cassette	↓	ACTC1	Actin	P68032	↓	adenine	C00147	↑
	ADSL	Adenylosuccinate lyase	↓	ATP5B	ATP synthase	P06576	↓	adenosine	C00212	↑
	ATP1B1	ATPase	↓	BAT1	HLA-B	Q13838	↑	AMP	C00020	↑
	ENPP2	Phosphodiesterase 2	↓	DDX39	DEAD	O00148	↑	GMP	C00144	↑
	POLA2	DNA polymerase	↑	MYH1	Myosin	P12882	↓	Guanine	C00242	↑
	POLR3C	RNA polymerase III	↓	POLRMT	RNA polymerase	O00411	↓	Xanthine	C00385	↓
	SMARCA5	SWI/SNF related	↓	PSMC4	Proteasome	P43686	↓			
	TRAP1	TNF receptor-associated	↓	RUVBL2	RuvB-like 2	Q9Y230	↑			
Urea Cycle and Metabloism of Amino Groups	ACY1	aminoacylase 1	↓	GLUD1	Glutamate dehydrogenase 1	P00367	↓	Creatine	C00300	↑
	CKMT1B	creatine kinase, mitochondrial 1B	↓	GLUD2	Glutamate dehydrogenase 2	P49448	↓	L-glutamic acid	C00302	↑
								L-proline	C00148	↑
								Spermidine	C00315	↑
Pyrimidine Metabolism	DCTD	dCMP deaminase	↓	POLRMT	RNA polymerase	O00411	↓	beta-alanine	C00099	↑
	POLA2	DNA polymerase	↑	UMPS	Uridine monophosphate synthetase	P11172	↓	UMP	C00105	↑
	POLR3C	RNA polymerase III	↓					uridine	C00299	↑

To determine differential gene expression levels, microarray analyses were performed using Affymetrix human genome U95 arrays. Three independent experiments were performed in duplicate for each cell type. A total of 453 genes with >1.5 fold altered expression levels in ATCL8 cells, as compared to AT5BIVA cells, were selected at a false discovery rate ≤0.05 (Supplementary Table S2, Supporting Information). The nonfunctional status of ATM altered the molecular profile of A-T cells (AT5BIVA), as shown in multidimensional scaling (MDS) plots with respect to differentially expressed genes (Figure 2D). A subset of these genes were validated by quantitative-RTPCR (qRT-PCR) to confirm differential expression of SATB1, EPHB1, RELA, CDH11, HDAC1, MCL1, SLC16A4, CASP3 and GAS6 in ATCL8 as compared to AT5BIVA (Supplementary Figure S3, Supporting Information). Pathway analyses using DAVID showed a predominant representation of genes involved in cell proliferation and apoptosis, cell adhesion and migration, and response to stress (Supplementary Table S3, Supporting Information). The microarray data set was also uploaded in the IPA tool for functional pathway analysis.

Since two-dimensional (2D) gel based protein analysis provides insight into differential levels of protein as well as the change in the post-translational modification status, we determined the effects of ATM on differential protein expression under basal conditions, by resolving whole cell protein lysates using 2D gel electrophoresis (see Materials and Methods). The differentially expressed protein spots were identified using MALDI-TOF mass spectrometry. The data set consisting of 131 proteins showing a significant change in relative levels that were identified with a high protein identification score and had three or more unique peptides as identified through MALDI-TOF/TOF MS were uploaded in the IPA tool for functional pathway analysis which showed a predominant representation of proteins involved in regulating ILK and calcium signaling, purine and amino acid metabolism (Supplementary Figure S4A, Supporting Information). A subset of these proteins is listed in Supplementary Table S4A, Supporting Information. The network analysis of the proteomics data set revealed seven major network modules (Supplementary Table 4B, Supporting Information). These included networks regulating a variety of cellular processes including cell cycle, proliferation, DNA repair, replication, protein modification and nucleic acid metabolism among others. Supplementary Figure S4B (Supporting Information) represents a network of molecules like BAT1[22] and HAUS1[23] predicted to be participating in cell division while HSP90 has been shown to be involved in DNA damage response following radiation exposure.[24] CBR1 and 3 are members of the carbonyl reductase family, predicted to be involved in the NRF2 mediated oxidative stress response.[25]

In order to integrate these "3-omics" information, the proteomics and microarray data sets were scored for differentially expressed proteins or genes participating in dysregulated metabolic pathways using the IPA tool. The data integration across all three levels of expression showed an excellent correlation for purine, pyrimidine and urea cycle metabolism pathways (Table 1 and Supplementary Figure S5, Supporting Information). The genes participating in these pathways were validated using qRTPCR (Supplementary Figure S6, Supporting Information). The selected features representing small molecule metabolites were subsequently validated by comparing MS/MS fragmentation patterns and retention times of the target ion and the standard metabolite (Figure 3A, Supplementary Figure S7A-K and Supplementary Table S4, Supporting Information). In addition,

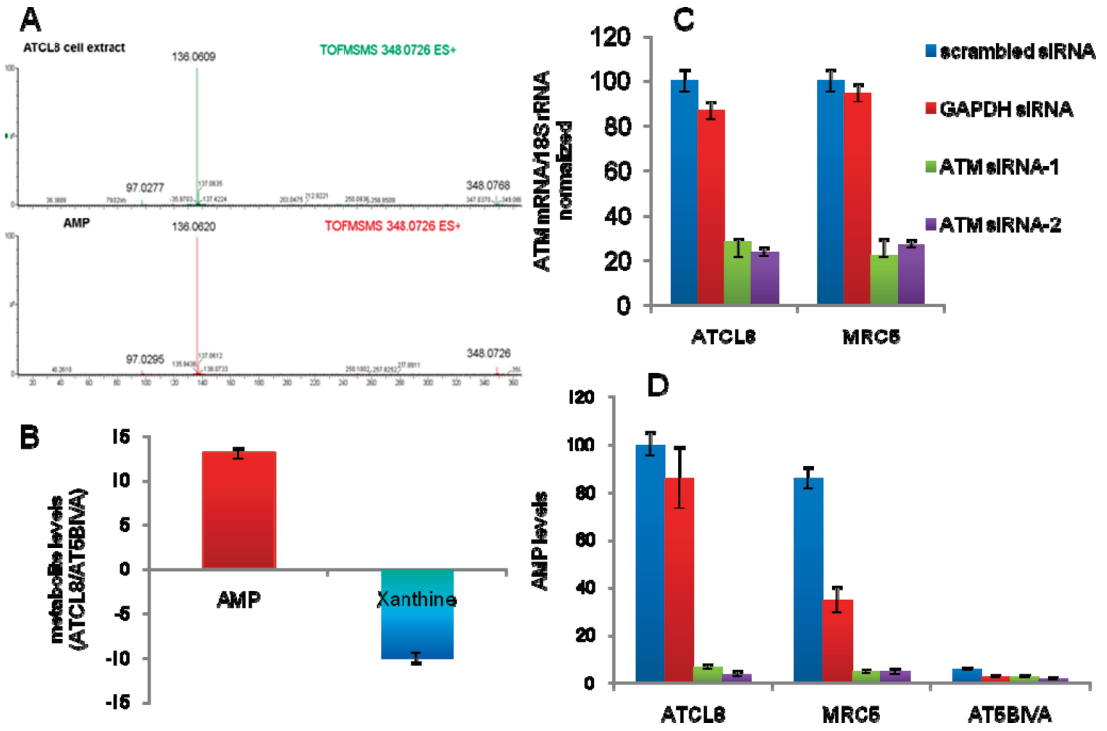

Figure 3. Deregulation of AMP and xanthine levels in AT5BIVA cell line. A. Determination of the chemical structure of an upregulated metabolite in ATCL8 by tandem mass spectrometry. Top panel shows the positive ion MS/MS fragmentation of the m/z 348.0705 from ATCL8 cell extracts. The bottom panel shows the positive ion mode fragmentation spectra for synthetic adenosine 3′ monophosphate (AMP) B. Semiquantitative analysis of AMP and Xanthine in ATCL8 as compared to AT5BIVA cells C. Quantitation of ATM mRNA by qRTPCR in ATCL8 and MRC5CV1 control cells, treated with GAPDH siRNA and ATM siRNA D. Mass spectrometry based quantitation of AMP levels under the same conditions.

some of the metabolites including β-alanine were cross validated by GC-MS profiling.

A remarkable finding was presented by the observed deregulation of metabolites belonging to the purine metabolism pathway (Supplementary Figure S8, Supporting Information). Levels of AMP were 13-fold increased, while levels of xanthine were 10-fold decreased in ATCL8 as compared to AT5BIVA cells (Figure 3B). Previous reports have linked increased intracellular concentrations of xanthine to ongoing oxidative stress and increased ROS production in A-T cells.[26] It has also been reported that increased levels of xanthine are accompanied by decreased AMP levels. To confirm that intracellular AMP levels are dependent on ATM function, ATM knockdown was performed in ATCL8 and MRC5CV1 (control) cells using ATM siRNA (Figure 3C). Subsequently, relative quantitation of AMP levels using UPLC−TOF MS showed a significant decrease in AMP levels in ATM knock-down ATCL8 and MRC5CV1 as compared to cells treated with scrambled or GAPDH siRNA (Figure 3D). These data support a direct correlation between ATM levels and intracellular AMP levels. Our data highlight imbalance in AMP/xanthine levels as a major characteristic of ATM-deficient cells.

That AMP levels were decreased in AT5BIVA cells and restored in ATCL8 cells to levels comparable to that of normal fibroblasts is pertinent to cellular energy metabolism. Increased AMP levels are known to activate 5′-AMP -activated protein kinase (AMPK), a major sensor and regulator of cellular energy homeostasis.[27] Hence we hypothesized that low AMP levels in AT5BIVA cells are unable to activate AMPK, consistent with a mechanism leading to defects in metabolism (i.e., insulin resistance). AMPK activity is known to be allosterically stimulated by the binding of AMP to the gamma subunit of AMPK making it a more attractive substrate for the upstream AMPK kinases that phosphorylate AMPK subunit alpha on threonine 172 (Thr172). Surprisingly, we found that AMPK was constitutively phosphorylated on Thr172 in AT5BIVA as well as two other A-T cell lines but not in ATCL8 cells (Supplementary Figure S9A, Supporting Information). As a cellular energy sensor responding to low ATP levels, AMPK activation positively regulates signaling pathways that replenish cellular ATP supplies. Following activation, catabolic pathways such as fatty acid oxidation and glycolysis are activated while ATP-consuming pathways such as lipogenesis are switched off. This is due to the short-term effects on phosphorylation of regulatory proteins such as acetyl CoA carboxylase (ACC) and by long-term effects on gene expression, for example Glutamate transporter (GLUT4). We further found that phosphorylated AMPK enhances the GLUT4 transcription and ACC phosphorylation in AT5BIVA cells demonstrating constitutive activation of the AMPK signaling pathway in ATM-deficient cells (Supplementary Figure S9B and C, Supporting Information). However, the levels of ATP were 1.6 fold increased in AT5BIVA cells as compared to ATCL8 (Supplementary Figure S9D).[28,29] Thus, the decrease in the intracellular levels of AMP in AT5BIVA may reflect rapid turnover of this metabolite for conversion into ATP as a consequence to constitutive AMPK activation resulting in disruption of a normal metabolism flow.

CONCLUSION AND FUTURE WORK

In conclusion, an integrated systems approach has revealed common links at the mRNA, protein and small molecule metabolite level, for purine, pyrimidine and energy metabolism. Since a diseased state can be perceived as a perturbation of cellular pathways, this approach can be effectively used for linking

the network modifications to overall physiological status. This work addresses basal transcription leading to the identification of genes and metabolic pathways not previously attributed to the basal function of ATM, and offering significance for the clinical phenotype. This may be expected to position cells for differential phenotypic responses to external stresses depending on the functional status of ATM. Future improvements in metabolite databases and improved gene-metabolite assignments will allow more robust metabolites identifications for better correlation of cross platform data.

■ ASSOCIATED CONTENT

Supporting Information

Supplemental figures and tables. This material is available free of charge via the Internet at http://pubs.acs.org.

■ AUTHOR INFORMATION

Corresponding Author

*Amrita K. Cheema, PhD Assistant Professor, Department of Oncology, Lombardi Comprehensive Cancer Center GD9, Pre Clinical Science Building, 3900 Reservoir Road NW, Washington D.C. 20057. E-mail: akc27@georgetown.edu. Phone: (202)687-2756. Fax: (202)687-8860.

Author Contributions

†These authors contributed equally to this work.

■ ACKNOWLEDGMENT

This work was supported in part by NIH grants PO1CA74175 and 2P30CA51008. We thank Alfredo Velena, Sung Lee, Theresa Carr, Jenny Tuturea, Xueping Zhang and Lihua Zhang for technical assistance. We also thank Dr. Albert J Fornace Jr. for scientific discussions and critical reading of the manuscript.

■ REFERENCES

(1) Dieterle, F.; Riefke, B.; Schlotterbeck, G.; Ross, A.; Senn, H.; Amberg, A. NMR and MS methods for metabonomics. *Methods Mol. Biol.* **2011**, *691*, 385–415.

(2) Mamas, M.; Dunn, W. B.; Neyses, L.; Goodacre, R. The role of metabolites and metabolomics in clinically applicable biomarkers of disease. *Arch Toxicol.* **2011**, *85*, 5–17.

(3) Kell, D. B. Metabolomics and systems biology: making sense of the soup. *Curr. Opin. Microbiol.* **2004**, *7* (3), 296–307.

(4) Fukushima, A.; Kusano, M.; Redestig, H.; Arita, M.; Saito, K. Integrated omics approaches in plant systems biology. *Curr. Opin. Chem. Biol.* **2009**, *13* (5−6), 532–8.

(5) Kell, D. B. Systems biology, metabolic modelling and metabolomics in drug discovery and development. *Drug Discovery Today* **2006**, *11* (23−24), 1085–92.

(6) del Sol, A.; Balling, R.; Hood, L.; Galas, D. Diseases as network perturbations. *Curr Opin Biotechnol.* **2010**, *21* (4), 566–71.

(7) Reaves, M. L.; Rabinowitz, J. D. Metabolomics in systems microbiology. *Curr Opin Biotechnol.* **2010**; DOI:10.1016/j.copbio.2010.10.001.

(8) Boder, E., Ataxia-Telangiectasia: An Overview. In *Ataxia-Telangiectasia: Genetics, Neuropathology and Immunology of a degenerative Disease of Childhood*; Richard, A., Gatti, M. S. L., Ed.; New York, 1985; pp 1−63.

(9) Cunliffe, P. N.; Mann, J. R.; Cameron, A. H.; Roberts, K. D.; Ward, H. W. C. Radiosensitivity in ataxia-telangiectasia. *Br. J. Radiol.* **1975**, *48* (569), 374–76.

(10) Taylor, A.; Metcalfe, J.; Thick, J.; Mak, Y. Leukemia and lymphoma in ataxia telangiectasia. *Blood* **1996**, *87* (2), 423–38.

(11) Swift, M.; Morrell, D.; Massey, R. B.; Chase, C. L. Incidence of cancer in 161 families affected by ataxia-telangiectasia. *N. Engl. J. Med.* **1991**, *325* (26), 1831–6.

(12) Savitsky, K.; Bar-Shira, A.; Gilad, S.; Rotman, G.; Ziv, Y.; Vanagaite, L.; Tagle, D. A.; Smith, S.; Uziel, T.; Sfez, S.; Ashkenazi, M.; Pecker, I.; Frydman, M.; Harnik, R.; Patanjali, S. R.; Simmons, A.; Clines, G. A.; Sartiel, A.; Gatti, R. A.; Chessa, L.; Sanal, O.; Lavin, M. F.; Jaspers, N. G.; Taylor, A. M.; Arlett, C. F.; Miki, T.; Weissman, S. M.; Lovett, M.; Collins, F. S.; Shiloh, Y. A single ataxia telangiectasia gene with a product similar to PI-3 kinase. *Science* **1995**, *268* (5218), 1749–53.

(13) Lavin, M. F. Ataxia-telangiectasia: from a rare disorder to a paradigm for cell signalling and cancer. *Nat. Rev. Mol. Cell Biol.* **2008**, *9* (10), 759.

(14) Bakkenist, C. J.; Kastan, M. B. DNA damage activates ATM through intermolecular autophosphorylation and dimer dissociation. *Nature* **2003**, *421* (6922), 499–506.

(15) Zhan, H.; Suzuki, T.; Aizawa, K.; Miyagawa, K.; Nagai, R. Ataxia telangiectasia mutated (ATM)-mediated DNA damage response in oxidative stress-induced vascular endothelial cell senescence. *J Biol Chem* **2010**, *285* (38), 29662–70.

(16) Varghese, R. S.; Cheema, A.; Cheema, P.; Bourbeau, M.; Tuli, L.; Zhou, B.; Jung, M.; Dritschilo, A.; Ressom, H. W. Analysis of LC−MS data for characterizing the metabolic changes in response to radiation. *J. Proteome Res.* **2010**, *9* (5), 2786–93.

(17) Jung, M.; Zhang, Y.; Lee, S.; Dritschilo, A. Correction of radiation sensitivity in ataxia telangiectasia cells by a truncated I kappa B-alpha. *Science* **1995**, *268* (5217), 1619–21.

(18) Dennis, G., Jr.; Sherman, B. T.; Hosack, D. A.; Yang, J.; Gao, W.; Lane, H. C.; Lempicki, R. A. DAVID: Database for Annotation, Visualization, and Integrated Discovery. *Genome Biol.* **2003**, *4* (5), 3.

(19) Kathryn Sheikh, S. W. B.; Fornace, A. J., Jr.; Cheema, A. K. Small molecule metabolite extraction strategy for improving LC/MS detection of cancer cell metabolome. *J. Biomol. Tech.* **2011**in press.

(20) Lee, S. J.; Dimtchev, A.; Lavin, M. F.; Dritschilo, A.; Jung, M. A novel ionizing radiation-induced signaling pathway that activates the transcription factor NF-kappaB. *Oncogene* **1998**, *17* (14), 1821–6.

(21) Breiman, L. Random Forests. *Machine Learning* **2001**, *45*, 5–32.

(22) Colon, M.; Hernandez, F.; Lopez, K.; Quezada, H.; Gonzalez, J.; Lopez, G.; Aranda, C.; Gonzalez, A. Saccharomyces cerevisiae Bat1 and Bat2 Aminotransferases Have Functionally Diverged from the Ancestral-Like Kluyveromyces lactis Orthologous Enzyme. *PLoS ONE* **2010**, *6* (1), e16099.

(23) Goshima, G.; Mayer, M.; Zhang, N.; Stuurman, N.; Vale, R. D. Augmin: a protein complex required for centrosome-independent microtubule generation within the spindle. *J. Cell Biol.* **2008**, *181* (3), 421–9.

(24) Dote, H.; Burgan, W. E.; Camphausen, K.; Tofilon, P. J. Inhibition of hsp90 compromises the DNA damage response to radiation. *Cancer Res.* **2006**, *66* (18), 9211–20.

(25) Hubner, R. H.; Schwartz, J. D.; De Bishnu, P.; Ferris, B.; Omberg, L.; Mezey, J. G.; Hackett, N. R.; Crystal, R. G. Coordinate control of expression of Nrf2-modulated genes in the human small airway epithelium is highly responsive to cigarette smoking. *Mol. Med.* **2009**, *15* (7−8), 203–19.

(26) Barzilai, A.; Rotman, G.; Shiloh, Y. ATM deficiency and oxidative stress: a new dimension of defective response to DNA damage. *DNA Repair (Amst)* **2002**, *1* (1), 3–25.

(27) Hardie, D. G. AMP-activated/SNF1 protein kinases: conserved guardians of cellular energy. *Nat. Rev. Mol. Cell Biol.* **2007**, *8* (10), 774–85.

(28) Hardie, D. G. AMPK: a key regulator of energy balance in the single cell and the whole organism. *Int. J. Obes. (London)* **2008**, *32* (Suppl 4), S7–12.

(29) Carling, D.; Sanders, M. J.; Woods, A. The regulation of AMP-activated protein kinase by upstream kinases. *Int. J. Obes. (London)* **2008**, *32* (Suppl 4), S55–9.